Multipoles model for $K^+\Lambda$ photoproduction on the nucleon reexamined

T. Mart* and S. Sakinah
Departemen Fisika, FMIPA, Universitas Indonesia, Depok 16424, Indonesia
(Received 2 February 2017; published 25 April 2017)

We have updated our previous multipoles model for the kaon photoproduction process $\gamma p \to K^+\Lambda$ by using the recently available experimental data, including the new CLAS 2016 data, and up-to-date information on the nucleon resonance properties provided by the Particle Data Group (PDG). The background and resonance parameters are extracted by fitting the calculated observables to nearly 7400 experimental data points and constraining the resonance parameters within the PDG error bars. The model can nicely reproduce the experimental data with $\chi^2/N_{\rm dof} = 1.63$. Different from the previous result, the present analysis finds the $N(1650)S_{11}$, $N(1720)P_{13}$, and $N(1900)P_{13}$ states to be the most important resonances in the process. Excluding these states in the model increases the value of χ^2 tremendously. As in our previous model, however, the contribution of the $N(1710)P_{11}$ state in minimizing χ^2 is found to be less significant. By including the new CLAS 2016 data in the fitting database and refitting the calculated observables to nearly 9000 data points, the $\chi^2/N_{\rm dof}$ increases to 2.88. In spite of the increase of χ^2, the agreement of model calculations with the new data is improved and the conclusion on the most important resonances in the process remains the same. An extensive comparison between the result of model calculations and experimental data on differential cross section, single polarization observables P, T, and Σ, as well as double polarization observables C_x, C_z, $O_{x'}$, $O_{z'}$, O_x, and O_z, is presented in this paper.

DOI: 10.1103/PhysRevC.95.045205

I. INTRODUCTION

More than a decade ago we proposed a phenomenological model for photoproduction on the nucleon, $\gamma p \to K^+\Lambda$, constructed from the covariant Feynman diagrams for the background terms and Breit–Wigner multipole amplitudes for the nucleon resonance terms [1]. Depending on the chosen data set, the number of data points in the fitting database was between 834 and 2444. Although much smaller compared to the present database, the number of data analyzed in our previous work [1] is obviously much larger than that used in Kaon–Maid [2]. Nonetheless, the result of our previous work was plagued by the problem of data consistency. As discussed in Ref. [1] and references therein, the differential cross section of SAPHIR data [3] is systematically smaller than that of CLAS data [4] at the total c.m. energy $W \gtrsim 1.7$ GeV. Since coupling constants in the background terms and Breit–Wigner parameters in the resonance terms were extracted from fitting to the data, three possible solution were proposed, depending on the data set used, i.e., including the SAPHIR data and excluding the CLAS data, excluding the SAPHIR data and including the CLAS data, or including both SAPHIR and CLAS data.

Now, a decade later, the number of experimental data points has increased to nearly 9000 which are dominated by the differential cross-section data. Statistically, the problem of data consistency has been remedied. The CLAS Collaboration has repeated the experiment and obtained a consistent result [5]. On the other hand, a newer measurement of differential cross section has been performed by utilizing the Crystal Ball detector at MAMI-C [6]. Although the measurement was performed only up to $W \approx 1.9$ GeV, the obtained data are more consistent to the CLAS data rather than the SAPHIR data. The same phenomenon is also shown by the LEPS data [7]. Therefore, in the present investigation we exclude the SAPHIR differential cross-section data [3] from our database.

Another important point to note is the use of nucleon resonances and their properties in the model which are adopted from the Particle Data Group (PDG) listing. In the previous work we used 16 out of 21 nucleon resonances listed in the 2004 RPP [8]. In the recent 2016 RPP the number of listed nucleon resonances has increased to 27 [9]. The quoted resonance properties in the recent RPP clearly originate from recent and up-to-date coupled-channels studies.

As seen in the following sections, the previous model fails to reproduce most of the new experimental data. Furthermore, in our previous work the resonance parameters were treated as free parameters in the fitting process. Therefore, most of the extracted parameters differ significantly from the PDG values. In the present work we use the PDG values as our starting point and, wherever it is possible, we constrain the values within the PDG uncertainties during the fit process. Based on the the conditions above, we believe that the update to our previous multipoles model [1] explained in the present paper is urgently required and timely. A short preliminary result of this work has been presented in a conference [10].

The organization of this paper is as follows: In Sec. II we present the formalism required in our model. Section III explains the nucleon resonances included in the model along with the experimental data used in the fitting database. In Sec. IV we present and discuss the result of our calculation. Here we compare the result obtained in the present work with the prediction of our previous works [1,11], since our motivation is eventually to replace the Kaon–Maid [2] with a better model. Section V is devoted to discuss the effect of new

*terry.mart@sci.ui.ac.id

CLAS 2016 data in the present model. Finally, in Sec. VI we summarize and conclude our findings.

II. FORMALISM

In general, we use the same formalism as in our previous work [1]. Since the number of nucleon resonances in the present work is larger, a number of modifications are certainly needed. These modifications can be found in our recent study for the $K\Sigma$ channels [12]. Nevertheless, in order to explain the extracted parameters discussed in Sec. IV we need to present the formula of Breit–Wigner parametrization for the resonances, i.e. [1,12,13],

$$A_{\ell\pm}(W) = \bar{A}_{\ell\pm} c_{K\Lambda} \frac{f_{\gamma R}(W)\Gamma_{\rm tot}(W) M_R f_{KR}(W)}{M_R^2 - s - i M_R \Gamma_{\rm tot}(W)} e^{i\phi}, \quad (1)$$

where M_R is the physical mass of resonance, $\Gamma_{\rm tot}$ is the resonance total width, $\bar{A}_{\ell\pm}$ represents the electric or magnetic multipoles photon couplings, $c_{K\Lambda}$ is the isospin factor, f_{KR} is the Breit–Wigner factor, $f_{\gamma R}$ indicates the contribution of the γNR vertex to the electric and magnetic multipoles, and ϕ

TABLE I. The nucleon resonances used in the present work along with their properties. The helicity amplitudes $A_{1/2}$ and $A_{3/2}$ of both proton and neutron are given in units of 10^{-3} GeV$^{-1/2}$. Unless stated in the footnote, data are estimates of the Particle Data Group in the Review of Particle Properties [15].

State	M_R (MeV)	Γ_R (MeV)	β_K ($\times 10^{-3}$)	$A_{1/2}(p)$	$A_{3/2}(p)$	$A_{1/2}(n)$	$A_{3/2}(n)$	Overall status	Status in $K\Lambda$
$N(1650)S_{11}$	1645 to 1670	104 ± 10[a]	100 ± 50[a]	55 ± 30[b]		−50 ± 20		****	***
$N(1895)S_{11}$	1895 ± 15[a]	95 ± 30[c]	180 ± 50[a]	12 ± 6[a]		3 ± 7[b]		**	**
$N(1710)P_{11}$	1680 to 1740	368 ± 120[d]	50 ± 30[d]	40 ± 20		−40 ± 20		***	***
$N(1880)P_{11}$	1875 ± 40[e]	235 ± 65[a]	20 ± 10[a]	14 ± 3[a]		14 ± 7[b]		**	*
$N(2300)P_{11}$	$2300^{+40+109}_{-30}$[f]	340 ± 30^{+110}_{-58}[f]						**	
$N(1720)P_{13}$	1700 to 1750	150 to 400	43 ± 4[d]	110 ± 45[a]	150 ± 30[a]	7 ± 15[g]	−5 ± 25[g]	****	**
$N(1900)P_{13}$	1915 ± 60[h]	270 ± 50[e]	0 to 100	26 ± 15[a]	−65 ± 30[a]	−10 ± 4[i]	−11 ± 7[i]	***	***
$N(1700)D_{13}$	1650 to 1750	100 to 250		15 ± 25	−15 ± 25	20 ± 15	−30 ± 20	***	*
$N(1875)D_{13}$	1820 to 1920	857 ± 100[d]	2 ± 2[j]	18 ± 10[a]	−9 ± 5[a]	10 ± 10	−20 ± 15	***	***
$N(2120)D_{13}$	2150 ± 60[a]	330 ± 45[a]		125 ± 45[a]	150 ± 60[a]			**	**
$N(1675)D_{15}$	1670 to 1680	120 ± 15[c]		21 ± 11[k]	15 ± 9[k]	−60 ± 5	−85 ± 19	****	*
$N(2060)D_{15}$	2060 ± 15[a]	400 ± 100[l]	30 ± 20[a]	65 ± 12[a]	55^{+15}_{-35}[a]	−12 ± 17[i]	−23 ± 23[i]	**	
$N(2570)D_{15}$	2570^{+19+34}_{-10-10}[f]	250^{+14+69}_{-24-21}[f]						**	
$N(1680)F_{15}$	1680 to 1690	118 ± 6[a]		−13 ± 3[a]	133 ± 12	29 ± 10	−33 ± 9	***	
$N(1860)F_{15}$	1820 to 1960	95 ± 20[c]	10[i]	20 ± 12[a]	50 ± 20[a]	10 ± 5[i]	−9 ± 5[i]	**	
$N(2000)F_{15}$	1950 to 2150	460 ± 100[a]		35 ± 15[a]	50 ± 14[a]			**	**
$N(1990)F_{17}$	1970 ± 50[l]	350 ± 120[l]		42 ± 14[a]	58 ± 12[a]	−1[m]	−178[m]	**	
$N(2190)G_{17}$	2100 to 2200	270 ± 50[n]	5 ± 3[a]	−65 ± 8[a]	35 ± 17[a]			****	*
$N(2250)G_{19}$	2200 to 2350	230 to 800		10[a]	10[a]			****	
$N(2220)H_{19}$	2200 to 2300	350 to 500		10[a]	10[a]			****	
$N(2600)I_{1,11}$	2550 to 2750	900 ± 100[c]						***	
$N(2700)K_{1,13}$	2612 ± 45[c]	900 ± 150[c]						***	

[a]Taken from Ref. [16], not a PDG estimate.
[b]Taken from Ref. [17], not a PDG estimate.
[c]Taken from Ref. [18], not a PDG estimate.
[d]Taken from Ref. [19], not a PDG estimate.
[e]Taken from Ref. [20], not a PDG estimate.
[f]Taken from Ref. [21], not a PDG estimate.
[g]Taken from Ref. [22], not a PDG estimate.
[h]Taken from Ref. [23], not a PDG estimate.
[i]Taken from Ref. [24], not a PDG estimate.
[j]Taken from Ref. [25], not a PDG estimate.
[k]Taken from Ref. [26], not a PDG estimate.
[l]Taken from Ref. [27], not a PDG estimate.
[m]Taken from Ref. [28], not a PDG estimate.
[n]Taken from Ref. [21], not a PDG estimate.

measures the resonance phase. A detailed explanation of these parameters can be found in Refs. [1,12,13].

In the resonance part the fitted parameters include the physical resonance mass M_R, the resonance width Γ_R, the single-kaon branching ratio β_K, the photon helicity amplitudes $A_{1/2}$ and $A_{3/2}$, and the resonance phase ϕ. The relations between the resonance width Γ_R, the single-kaon branching ratio β_K, and the Breit–Wigner factor f_{KR} in Eq. (1) can be found in Eqs. (4), (5), and (7) of Ref. [1]. The relation between photon helicity amplitudes and electric or magnetic multipoles $\bar{A}_{\ell\pm}$ given in Eq. (1) is listed in Table I of Ref. [1].

In the background part the fitted parameters are the hadronic coupling constants and the hadronic form-factor cutoff Λ_B. As in our previous works [1,12] the values of the leading coupling constants, $g_{K\Lambda N}$ and $g_{K\Sigma N}$, are only allowed to vary within the SU(3) prediction with 20% symmetry breaking [14].

III. NUCLEON RESONANCES AND EXPERIMENTAL DATA

Although the number of data considered in the present work is larger than that in the $K\Sigma$ photoproduction [12], the number of resonances included in the model is much smaller because Δ resonances cannot contribute due to the isospin conservation at hadronic vertex. Furthermore, by excluding the resonance with one-star rating in the overall status as reported by the Particle Data Group (PDG) in the Review of Particle Properties (RPP) [15], the number of included nucleon resonances reduces to only 22. These resonances along with their properties obtained from PDG listing [15] and other sources are listed in Table I. Note that we start with the 2014 RPP [15], since we need to discuss the properties of a number of resonances available in this version, e.g., the $P_{11}(1710)$ and the narrow $P_{11}(1685)$ states, and to fairly compare the result obtained with the latest 2016 RPP [9]. In the case of other resonances, we observe that the difference between the the nucleon properties listed in the 2014 RPP [15] and 2016 RPP [9] does not substantially influence the present work.

The number of data points included in the present work is obviously larger than that of the previous study [1]. As shown in Table II we used only 1694 data points in the previous study, whereas the total number of data in the present work is nearly four times larger if the new CLAS 2016 data [29] are included. Note that, for the previous study, we refer to model Fit 2 of Ref. [1], which excludes the SAPHIR data [3] in its fitting database in order to make a fair comparison with the result of present work where we also exclude the SAPHIR data to avoid the problem of internal consistency in the cross section, as discussed in Introduction. Furthermore, in the present paper we do not discuss the model Fit 3 of Ref. [1], which was fit to both SAPHIR and CLAS data, because this model reproduces the average differential cross section and, therefore, does not reproduce both SAPHIR and CLAS differential cross section for $W \gtrsim 1.7$ GeV.

The present database is dominated by differential cross section and Λ recoil polarization data. This is natural because the two observables can be directly obtained from experiment. However, different from the previous database [1], the experimental error bars of recent data are much smaller. Furthermore, the present database contains more varieties of

TABLE II. Experimental data used in the present and previous analyses. See Ref. [1] and Sec. III for the explanation of data included in the previous analysis. In the present analysis Fit 1 and Fit 2 refer to the solutions that exclude and include the new SAPHIR 2016 data [29], respectively.

Collaboration	Observable	Symbol	N	Previous	Present		Reference
				Fit 2	Fit 1	Fit 2	
CLAS 2006	Differential cross section	$d\sigma/d\Omega$	1377	✓	✓	✓	[4]
	Recoil polarization	P	233	✓	✓	✓	[4]
CLAS 2010	Differential cross section	$d\sigma/d\Omega$	2066		✓	✓	[5]
	Recoil polarization	P	1707		✓	✓	[5]
Crystal Ball 2014	Differential cross section	$d\sigma/d\Omega$	1301		✓	✓	[6]
LEPS 2006	Differential cross section	$d\sigma/d\Omega$	54	✓	✓	✓	[7]
	Photon asymmetry	Σ	30	✓	✓	✓	[7]
GRAAL 2007	Recoil polarization	P	66		✓	✓	[30]
	Photon asymmetry	Σ	66		✓	✓	[30]
LEPS 2007	Differential cross section	$d\sigma/d\Omega$	12		✓	✓	[31]
CLAS 2007	Beam-recoil polarization	C_x	159		✓	✓	[32]
	Beam-recoil polarization	C_z	160		✓	✓	[32]
GRAAL 2009	Target asymmetry	Σ	66		✓	✓	[33]
	Beam-recoil polarization	$O_{x'}$	66		✓	✓	[33]
	Beam-recoil polarization	$O_{z'}$	66		✓	✓	[33]
CLAS 2016	Recoil polarization	P	314			✓	[29]
	Photon asymmetry	Σ	314			✓	[29]
	Target asymmetry	T	314			✓	[29]
	Beam-recoil polarization	O_x	314			✓	[29]
	Beam-recoil polarization	O_z	314			✓	[29]
Total				1694	7433	9003	

observables. The target asymmetry T and the beam-recoil double polarization observables C_x, C_z, O_x, O_z, $O_{x'}$, and $O_{z'}$ were not available in the previous analysis. From Table II it is also obvious that the number of photon asymmetry Σ data included in the present study is much larger and the data cover a wider kinematics.

We note that there are different sign conventions for polarization observables in the literature, especially when the recoil polarization is used. These different conventions are summarized in Table 1 of Ref. [34]. For the purpose of the present investigation the corresponding polarization observables are C_x, C_z, O_x, O_z, $O_{x'}$, and $O_{z'}$. Our convention for these observables is the same as the JLab-EBAC one [35,36]. In Ref. [11] a comparison between the result of JLab-EBAC model [36] and our previous covariant isobar model has been also discussed.

To conclude this section, in view of the number and quality of experimental data used in the present database, we believe that significant improvement in the model and our understanding of the involved resonances in kaon photoproduction would be expected from the present work.

IV. RESULTS AND DISCUSSION

The background parameters obtained from fitting the calculated observables to nearly 7400 experimental data points are listed in Table III, where the coupling constants and hadronic form-factor cutoff obtained from previous investigation are also displayed for comparison.

As in the previous analyses the leading coupling constants $g_{K\Lambda N}$ and $g_{K\Sigma N}$ were varied within the SU(3) prediction. The smaller value of hadronic cutoff Λ_B provides a clear indication that the background terms are strongly suppressed, even though we have used a larger number of hyperon resonances. Note that in the present model we also include the contribution of t-channel hyperon resonances in the background part, i.e., the $\Lambda(1405)$, $\Lambda(1600)$, $\Lambda(1670)$, $\Lambda(1800)$, $\Lambda(1810)$, $\Sigma(1600)$, and $\Sigma(1750)$. We observe that their coupling constants in the present model are relatively large. Nevertheless, the same phenomenon was also observed in the previous studies [12,37].

Contribution of the background terms to the total cross section is exhibited in Fig. 11 and will be discussed later in the next section. At this stage it is worth mentioning that this contribution is nearly ten times smaller than that found in our previous analysis (see Fig. 1 of Ref. [1]).

It was argued that the inclusion of certain hyperon [38] and kaon [especially the $K_1(1270)$ [39]] resonances can increase the values of leading coupling constants, closer to the SU(3) prediction. We believe, however, that the argument is only valid for a model with very few nucleon resonances and fitted to a small fraction of experimental data. With a large number of resonances and experimental data, presumably this argument is no longer valid, since contributions of the resonance tails in the whole range of energy are overlapping and large. As a consequence, the background terms must be significantly suppressed, by decreasing the value of Λ_B. Our previous works have shown that by carefully choosing the appropriate hadronic form factors and cutoffs the leading coupling constants can be fixed to the SU(3) value and the χ^2 can be further reduced [40]. However, we believe that this problem can be addressed in future investigations.

With an increase of 62 more parameters the χ^2 per number of degrees of freedom ($\chi^2/N_{\rm dof}$) also increases by nearly 65%. We believe that this result is still acceptable since the number of fitted data in the present work is more than four times larger than the number used in the previous one. Furthermore, since the error bars of recent data are much smaller than those of older ones, the calculated observables prefer to reproduce the recent data.

The extracted resonance parameters obtained in the present and previous analyses are given in Table IV. Unlike in the previous analysis, in the present one we have constrained the parameters within the uncertainties of PDG estimate [15], unless the values were not available from PDG or referred by PDG to other sources. In the latter, we used the referred values or we add 10% uncertainties to the referred values. Especially for the kaon branching ratio β_K, we put an upper limit of 10%, i.e., 0.100 in the fifth column of Table IV, if the value was not estimated by PDG.

Table IV reflects that we are able to constrain the resonance parameters in the kaon photoproduction process to the values obtained directly or indirectly from other reactions. This is important because, unlike in the coupled-channels formalism, in the single channel analyses the extracted resonance properties or coupling constants are usually considered as purely free parameters.

As in the previous work [1] we can define a parameter which measures the relative difference between the χ^2 obtained from fits using and excluding a certain resonance, i.e.,

$$\Delta\chi^2 = \frac{\chi^2_{\text{All}-N^*} - \chi^2_{\text{All}}}{\chi^2_{\text{All}}} \times 100\%, \tag{2}$$

where χ^2_{All} is the χ^2 obtained by using all resonances and $\chi^2_{\text{All}-N^*}$ is the χ^2 obtained by using all but a specific resonance. We have to emphasize here that the $\Delta\chi^2$ does not indicate the "coupling strength" of this resonance to the $K^+\Lambda$ channel, however it is merely used to estimate the difficulty of reproducing experimental data without this resonance.

We note that a similar ratio was also proposed in Ref. [42] in the framework of multichannel analysis and a more robust

TABLE III. Extracted background parameters and the hadronic cutoff Λ_B from fits to experimental data in the present and previous works. Note that $N_{\rm dof} = N_{\rm data} - N_{\rm par.}$.

Parameter	Present	Previous
$g_{K\Lambda N}/\sqrt{4\pi}$	− 3.00	− 3.80
$g_{K\Sigma N}/\sqrt{4\pi}$	1.30	1.20
$G^V_{K*}/4\pi$	− 0.10	0.06
$G^T_{K*}/4\pi$	− 0.04	− 0.18
$G^V_{K_1}/4\pi$	0.95	0.16
$G^T_{K_1}/4\pi$	0.41	− 1.13
Λ_B (GeV)	0.62	1.13
$N_{\rm data}$	7433	1694
$N_{\rm par.}$	141	79
$\chi^2/N_{\rm dof}$	1.63	0.98

TABLE IV. The nucleon resonance parameters extracted from fits to experimental data in the present and previous works. The values are comparable to the estimates of the PDG [15]; see Table I for details. The uncertainties in the extracted parameter values are merely obtained from MINUIT [41]. The last column is obtained by using Eq. (2).

Resonance (PDG status)	Data from	M_R (MeV)	Γ_R (MeV)	β_K (10^{-3})	$A_{1/2}(p)$ (10^{-3} GeV$^{-1/2}$)	$A_{3/2}(p)$ (10^{-3} GeV$^{-1/2}$)	ϕ (deg.)	$\Delta\chi^2$ (%)
$N(1650)S_{11}$	Present	1670 ± 0	114 ± 0	150 ± 5	66 ± 0		95 ± 1	49.0
(****)	Previous	1650 ± 0	150 ± 0	300 ± 283	3 ± 1		119 ± 22	0.1
$N(1895)S_{11}$	Present	1880 ± 0	125 ± 1	230 ± 63	14 ± 0		205 ± 2	3.9
(**)	Previous							
$N(1710)P_{11}$	Present	1680 ± 3	433 ± 18	20 ± 1	33 ± 1		167 ± 2	9.6
(***)	Previous	1720 ± 3	150 ± 5	10 ± 52	98 ± 4		191 ± 2	2.5
$N(1880)P_{11}$	Present	1915 ± 1	170 ± 1	30 ± 2	17		191 ± 3	5.4
(**)	Previous							
$N(2300)P_{11}$	Present	2281 ± 4	260 ± 15	11 ± 1	47 ± 2		266 ± 3	5.0
(**)	Previous							
$N(1720)P_{13}$	Present	1748 ± 2	309 ± 4	39 ± 0	75 ± 1	120 ± 0	191 ± 1	48.5
(***)	Previous	1720 ± 0	150 ± 0	97 ± 8	54 ± 3	−49 ± 2	136 ± 2	4.7
$N(1900)P_{13}$	Present	1974 ± 1	320 ± 1	100 ± 0	41	−88 ± 1	174 ± 0	76.7
(***)	Previous	1800 ± 5	500 ± 15	200 ± 10	69 ± 2	88 ± 1	208 ± 1	6.1
$N(1700)D_{13}$	Present	1650 ± 1	100 ± 2	10 ± 0	−10 ± 1	5 ± 1	360 ± 0	4.2
(***)	Previous	1750 ± 45	500 ± 385	10 ± 60	56 ± 4	93 ± 4	36 ± 2	3.6
$N(1875)D_{13}$	Present	1920 ± 9	757 ± 21	4 ± 0	15 ± 3	−14 ± 1	84 ± 6	3.8
(***)	Previous							
$N(2120)D_{13}$	Present	2163 ± 2	314 ± 4	8 ± 0	170 ± 1	90 ± 0	68 ± 1	10.9
(***)	Previous							
$N(1675)D_{15}$	Present	1680 ± 0	105 ± 0	46 ± 6	10 ± 0	10 ± 0	195 ± 1	4.6
(****)	Previous	1675 ± 0	150 ± 0	164 ± 29	−2 ± 0	−15 ± 1	212 ± 3	7.4
$N(2060)D_{15}$	Present	2045 ± 0	500 ± 8	13 ± 0	53 ± 3	70 ± 1	83 ± 2	13.5
(**)	Previous					−4		
$N(2570)D_{15}$	Present	2555 ± 4	333 ± 1	21 ± 1	−17 ± 1	39 ± 0	360 ± 1	5.6
(**)	Previous							
$N(1680)F_{15}$	Present	1690 ± 1	112 ± 9	0 ± 0	−16 ± 0	121 ± 20	86 ± 13	0.0
(**)	Previous	1680 ± 0	130 ± 0	0 ± 6	−17 ± 1	15 ± 1	5 ± 2	6.0
$N(1860)F_{15}$	Present	1954 ± 3	115 ± 3	8 ± 0	8 ± 0	70 ± 1	222 ± 2	10.7
(**)	Previous							
$N(2000)F_{15}$	Present	2150 ± 1	385 ± 18	6 ± 1	40 ± 1	36 ± 1	22 ± 3	3.0
(**)	Previous	1937 ± 4	153 ± 10	31 ± 5	53 ± 4	−14 ± 3	0 ± 17	4.5
$N(1990)F_{17}$	Present	1920 ± 1	470 ± 1	2 ± 0	28 ± 0	70 ± 1	251 ± 1	6.2
(**)	Previous	2083 ± 15	531 ± 10	300 ± 285	−12 ± 1	−15 ± 1	72 ± 3	8.0
$N(2190)G_{17}$	Present	2140 ± 3	220 ± 2	5 ± 0	−62 ± 3	43 ± 2	256 ± 2	6.4
(***)	Previous	2190 ± 0	450 ± 0	300 ± 272	−7 ± 1	14 ± 1	10 ± 3	4.9
$N(2250)G_{19}$	Present	2272 ± 15	438 ± 29	100 ± 4	0 ± 0	10 ± 0	165 ± 4	3.2
(****)	Previous	2250 ± 0	400 ± 0	300 ± 227	6 ± 1	3 ± 1	75 ± 7	1.9
$N(2220)H_{19}$	Present	2200 ± 1	500 ± 11	100 ± 1	−10 ± 0	10 ± 0	220 ± 1	6.6
(****)	Previous							
$N(2600)I_{1,11}$	Present	2750 ± 6	800 ± 26	5 ± 1	18 ± 3	−2 ± 0	111 ± 5	0.4
(***)	Previous							
$N(2700)K_{1,13}$	Present	2567 ± 1	1050 ± 8.6	100 ± 8	−5 ± 0	13 ± 0	225 ± 1	7.4
(**)	Previous							

mechanism to this end has been also proposed by using a Bayesian inference method in the single channel framework [43]. For the sake of simplicity and a fair comparison with the previous work, in the present study we use Eq. (2) and we need to mention that the conclusion drawn in Ref. [43] is qualitatively consistent with that of the present study.

The values of $\Delta\chi^2$ obtained from Eq. (2) in the present and previous works are listed in the last column of Table IV and pictorially displayed in Fig. 1. Obviously, the result of present study is completely different except for a number of resonances, e.g., the $N(1700)D_{13}$. By comparing the results of present and previous studies, the most striking ones are the $N(1650)S_{11}$, $N(1720)P_{13}$, and $N(1900)P_{13}$ states. Excluding one of these states in the model could raise the $\Delta\chi^2$ by up to ∼80%. Therefore, we might conclude that, according to the present study, the three resonances play important role in the

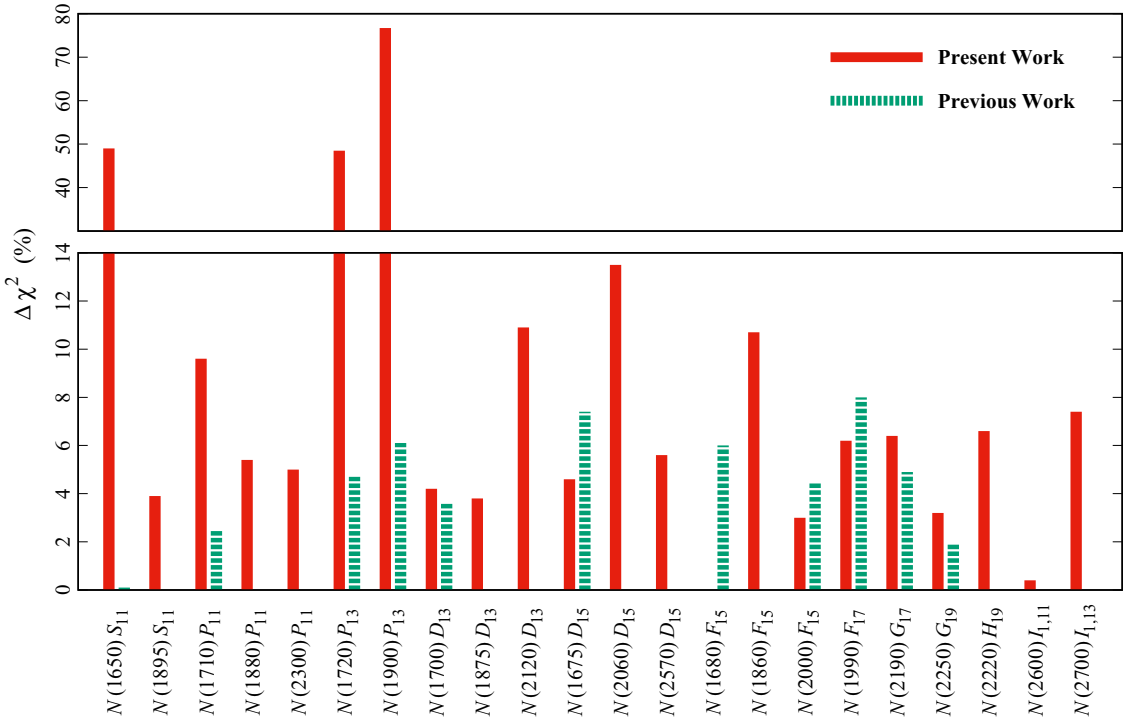

FIG. 1. The significance of individual resonances obtained in the present and previous [1] works. Note that not all resonances appeared in the horizontal axis were existing in the previous study.

kaon photoproduction process. The most dramatic one is of course the $N(1650)S_{11}$ resonance. In the previous study [1] we note that this resonance could become very important only if the SAPHIR data were included.

Figure 1 also indicates that the $N(1710)P_{11}$ resonance is slightly more important in the present study. This resonance has been raised from a three-star rating in the 2014 RPP [15] to a four-star rating in the 2016 RPP [9]. Nonetheless, compared to the $N(1720)P_{13}$ and $N(1900)P_{13}$ states, the $N(1710)P_{11}$ state is less important in both present and previous studies. The same finding is also reported in Ref. [44]. Figure 1 exhibits that the $N(1710)P_{11}$ is even less important than the $N(2120)D_{13}$, $N(2060)D_{15}$, and $N(1860)F_{15}$ states.

Finally, after comparing the values of $\Delta\chi^2$, obtained in the present and previous works shown in Fig. 1 we clearly observe that in the present work the level of significance of most resonances is higher than in the previous work. Since the number of resonances included in the present work is larger we would expect that, during the fitting process, the absence of a certain resonance would be compensated by the neighboring ones. Thus, in general, the level of significance of most resonances in the current study should be small. However, the number of data and observables used in the present fit are much larger than in the previous one. The data

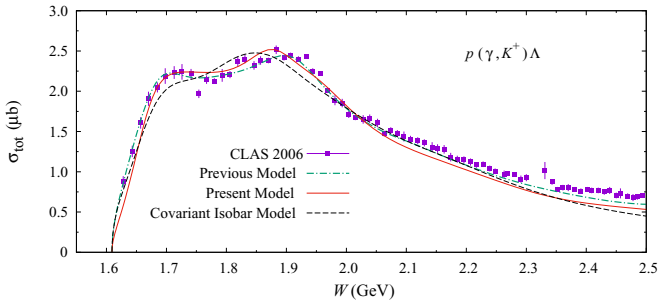

FIG. 2. Calculated total cross sections obtained from the previous multipoles model (dash-dotted line [1]), the covariant isobar model (dashed line [11]), and the present work (solid line). Experimental data taken from the CLAS Collaboration [4] are shown just for comparison and were not used during the fitting process.

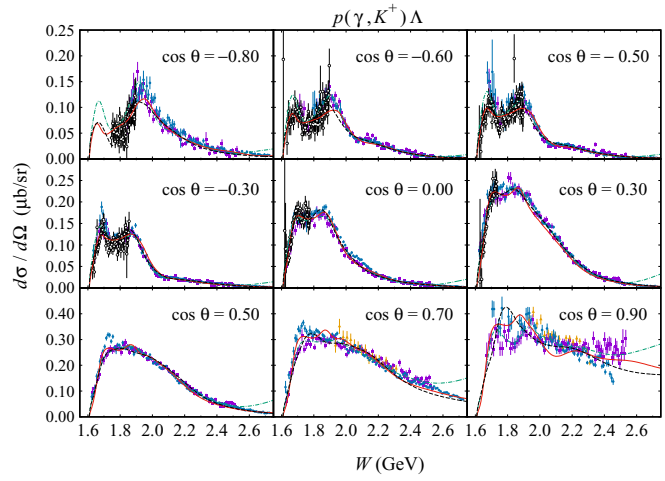

FIG. 3. Differential cross sections as a function of the total c.m. energy W for different values of the kaon c.m. angle. Experimental data are from the CLAS 2006 (solid squares [4]), CLAS 2010 (solid circles [5]), LEPS 2006 (solid triangles [7]), and Crystal Ball 2014 (open circles [6]) collaborations. Notation of the curves is as in Fig. 2.

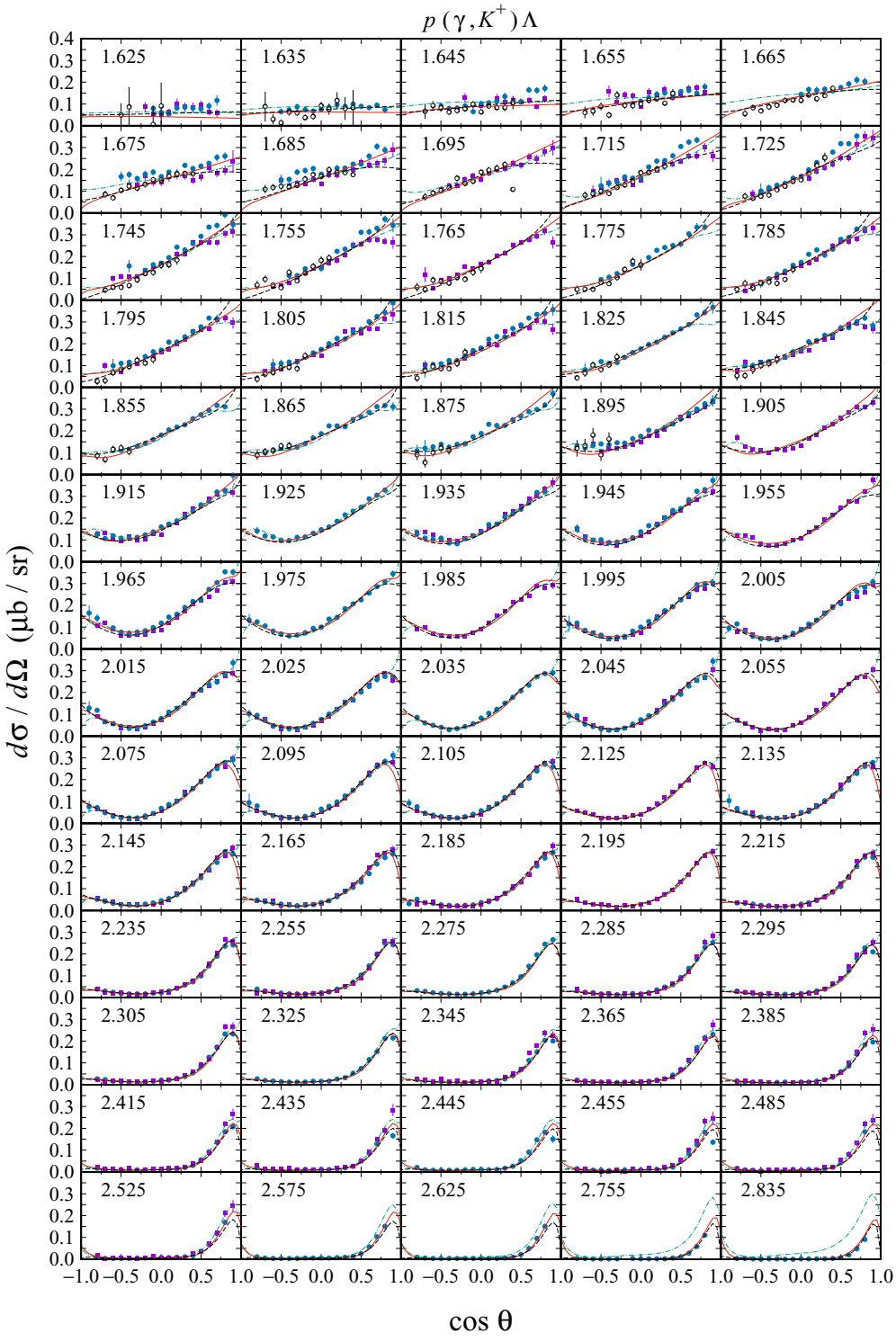

FIG. 4. As in Fig. 3, but for angular distributions.

also show a large number of structures, and to reproduce each of the structures a specific resonance seems to be required by the model. Therefore, the expected compensation by the neighboring resonances is not possible in this case.

Comparison between the total cross sections obtained in the present, previous multipoles [1], and previous covariant isobar [11] models, along with the CLAS 2006 experimental data [4] is shown in Fig. 2.

The previous covariant isobar model [11] is constructed from the covariant Feynman diagrams for both background and resonance parts. The background part is similar to that of the present work. The resonance part includes all nucleon

resonances listed in the PDG listing [15] with spins up to 5/2 and with at least two-star PDG rating. As a consequence, the number of included nucleon resonances is 17. The unknown coupling constants in both background and resonance terms are obtained from fitting to nearly 7400 experimental data points. Therefore, the main difference between the covariant isobar and the present models is in the resonance part. It is found that the use of consistent interaction [45] in both spin-3/2 and $-5/2$ nucleon resonances, i.e., model D of Ref. [11], leads to the best description of experimental data. In the following discussion we also use model D for comparison.

At first glance we might conclude that the previous multipoles model [1] works better than the recent covariant calculation [11] as well as the present study. This is in fact true for the case of CLAS 2006 experimental data. However, it should be noted that the previous multipoles model was fit to the data set dominated by the CLAS 2006 differential cross-section data [4], even though the total cross-section data shown by the solid squares in Fig. 2 were excluded from the database.

The smaller total cross sections at high energy shown by the results obtained in the present study and previous covariant isobar model presumably originate from the effect of CLAS 2010 and Crystal Ball 2014 differential cross-section data, as shown in Figs. 3 and 4. At high energies and forward angles the two data sets seem to be smaller than the CLAS 2006 one. Since the number of data points of the two data sets is much larger than that of the CLAS 2006 data, while the error bars are also smaller, the CLAS 2010 and Crystal Ball 2014 data have a stronger effect to decrease the cross sections at this kinematics. This is clearly shown in Fig. 3.

At low energies the differential cross-section data are more scattered and, therefore, the variation in the calculated cross section is large. Especially at very forward angles (Fig. 3 with $\cos\theta = 0.90$), where the three calculations display the largest variant. At this point we have to remind the reader that an accurate prediction of the cross section at forward angles is urgently required by the investigation of kaon photoproduction on nuclei [46] because only at this kinematics the nuclear cross sections are considerably large. In view of the results shown in Fig. 3 it is clear that in the future special effort should be devoted to study kaon photoproduction at forward angle in both theoretical and experimental sides

Another interesting phenomenon shown in Fig. 3 is the existence of sharp peaks at $W \approx 1.7$ GeV, which cannot be reproduced by the three models. From our experience an inclusion of a resonance with the mass of nearly 1.7 GeV and a relatively narrow width could help to relieve this problem. This could be a sign for the existence of a narrow resonance previously investigated in Refs. [47]. However, a careful investigation should be performed before we could draw such a conclusion, because a pronounced cusp could appear at this energy due to the opening channels (threshold energies) of the $K\Sigma$, ρp, and ωp photoproductions (see Refs. [47] for further explanation). Furthermore, we also observe that only the CLAS 2010 data show sharp peaks, whereas the CLAS 2006 and Crystal Ball 2014 data display relatively milder peaks.

The energy and angular distributions of recoil polarization observable P are shown in Figs. 5 and 6, respectively. For this observable we believe that the result of our present study

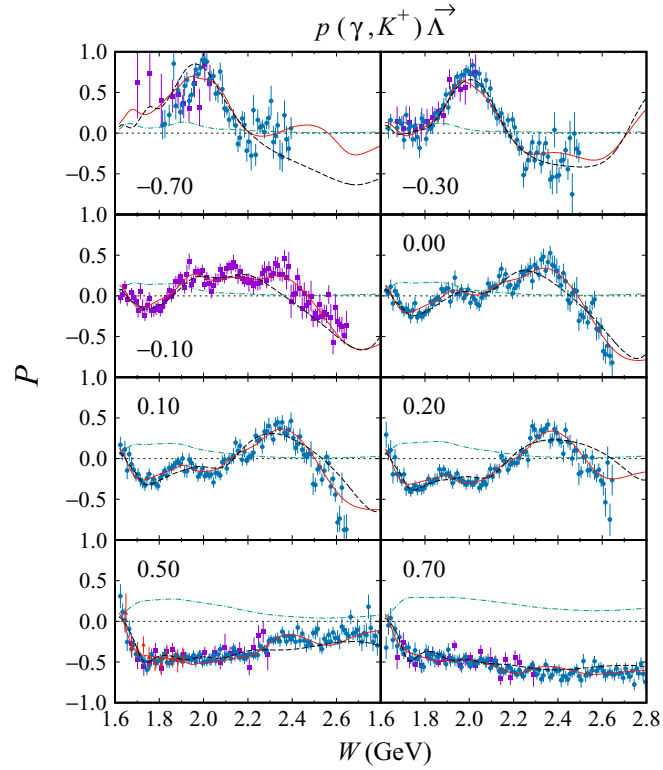

FIG. 5. Polarization of the recoiled Λ as a function of the total c.m. energy W for different values of $\cos\theta$, where θ is kaon angle in the c.m. system. Experimental data are from the CLAS 2006 (solid squares [4]), CLAS 2010 (solid circles [5]), and GRAAL 2007 (solid triangles [30]) collaborations. The corresponding value of $\cos\theta$ is given in each panel. Notation of the curves is as in Fig. 2.

is quite satisfactory, especially compared to the result of our previous multipoles model, which produces different sign of polarization at forward angles (see the two bottom panels of Fig. 6). The angular distribution of this polarization shown in Fig. 6 further exhibits that the present model yields an excellent agreement with experimental data.

Note that in Ref. [47] the evidence of a narrow resonance structure came from the recoil polarization P at $W \approx 1.65$ GeV. The structure is still visible in Fig. 6, where the CLAS 2010 data show a dip at this energy in the whole angular distributions. Although more data with different observables have been added in the present database and, as a consequence, the extracted model would probably become insensitive to this structure, a careful investigation of the narrow resonance indication at energy range between 1.61 and 1.72 GeV would be still relevant to resolve this issue. As discussed in Ref. [47], additional experimental data on recoil polarization from the JLab FROST project are urgently required to this end.

The calculated photon and target asymmetries are shown in Figs. 7 and 8, respectively. For these observables the agreement between model calculations and experimental data is, in general, fair, although at some kinematics it is good. In the low-energy region near the forward angles the present model displays some deficiencies. However, in the backward angle region as well as at high energies the agreement with experimental data is relatively good. The small number of

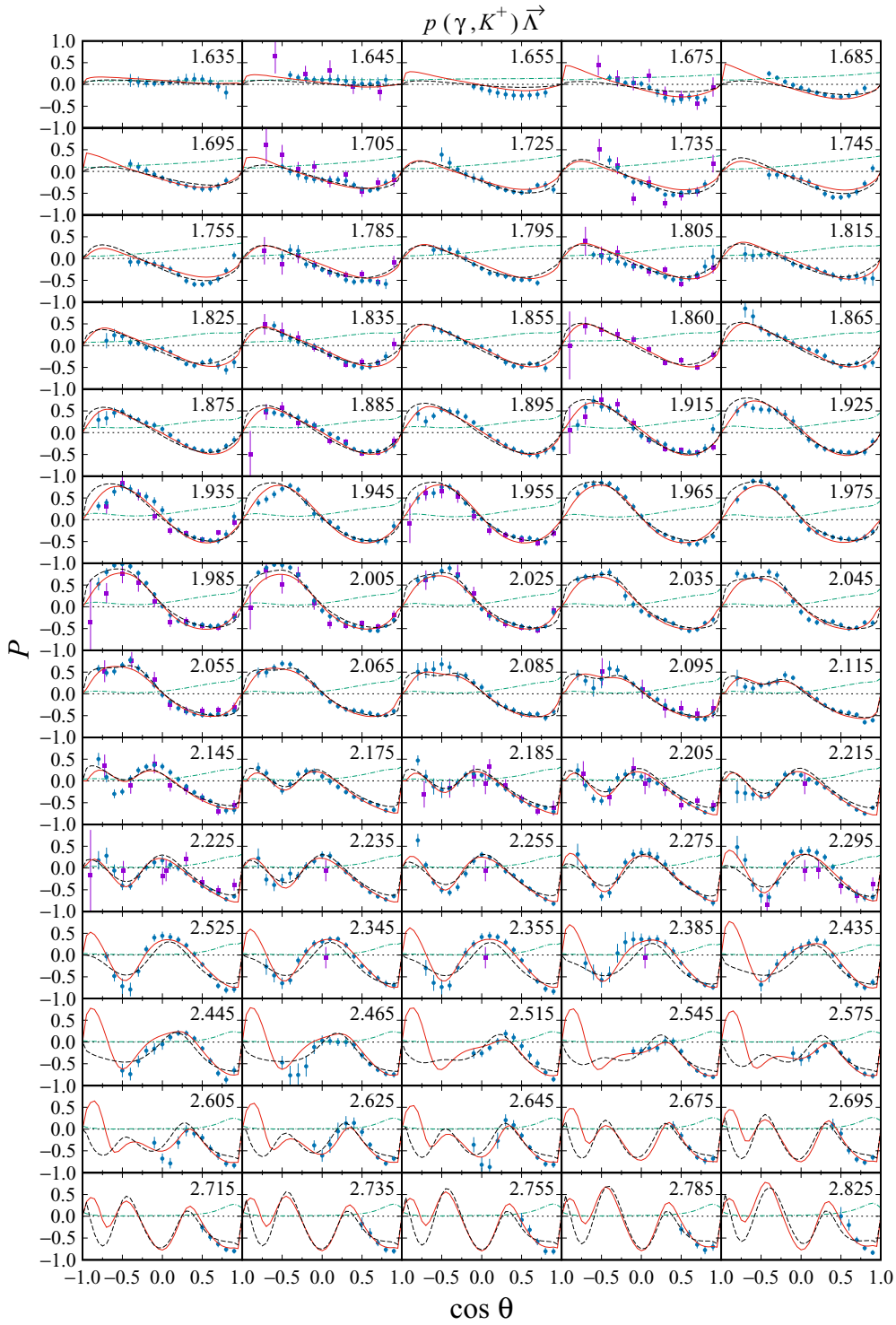

FIG. 6. As in Fig. 5, but for the angular distribution of the Λ recoil polarization with different values of the total c.m. energy W.

data of these observables could be the origin of this problem, since during the fitting process these data cannot compete with the differential cross section and recoil polarization data.

Unlike in the case of photon and target asymmetries, the experimental data on beam-recoil double polarization observables C_x and C_z can be nicely reproduced by the present model, as clearly shown in Fig. 9. At higher energies, however, we have to admit that there are some discrepancies with experimental data. Nevertheless, the error bars at this kinematics are also large. In general, the agreement between model calculation and experimental data for the C_x and C_z observables is much better than that for the photon and target asymmetries.

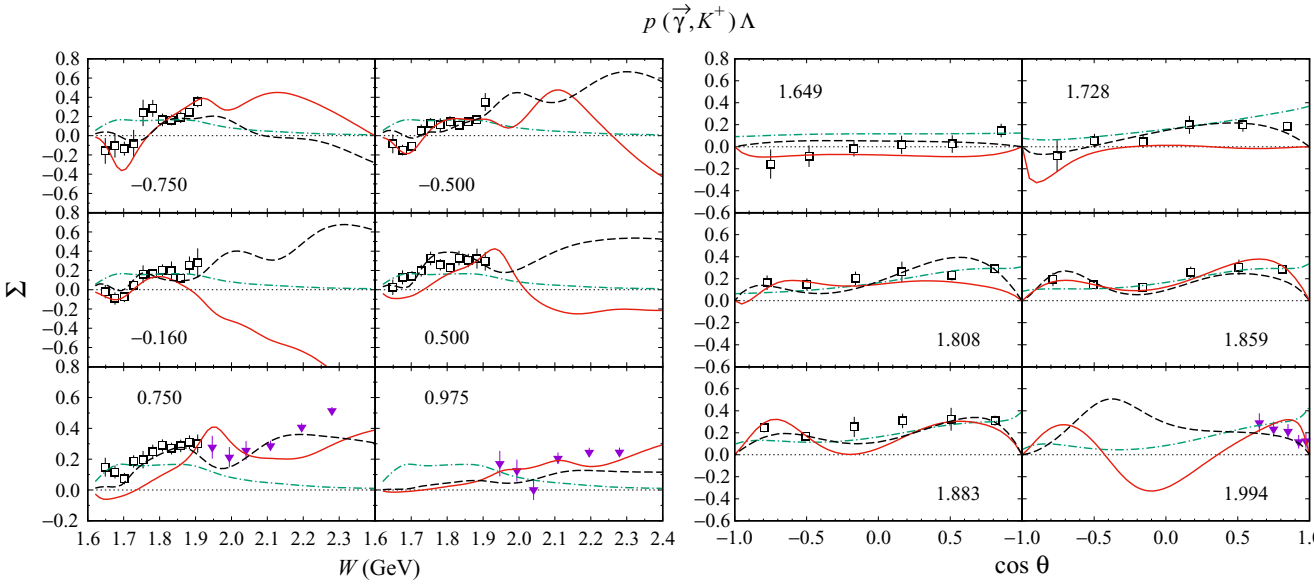

FIG. 7. Photon asymmetry as functions of the total c.m. energy and kaon angle. Notation of the curves is as in Fig. 2. Experimental data are from the GRAAL [30] (open squares) and LEPS [7] (open circles) collaborations.

Finally, the comparison between calculated beam-recoil double polarization observables $O_{x'}$ and $O_{z'}$ and experimental data are shown in Fig. 10. Although in this case the performance of our present model is better than in the case of photon and target asymmetries, a similar phenomenon appears again, i.e., the agreement with experimental data is better at backward angle and high-energy regions. Note that in both cases the problem appears if we compare the result of model calculation and the GRAAL data. The number of LEPS data is very small for the photon asymmetry, as such the data do not generate a big problem in the fit.

V. INCLUDING THE NEW CLAS DATA

Recently, we investigated the impact of including the new CLAS 2016 data [29] on the isobar model for $K\Sigma$ photoproduction [12]. This study was motivated by the fact that the prediction of Bonn–Gatchina model [48] showed significant discrepancy with the new data, as reported in Ref. [29]. It is also shown that the discrepancy can be removed after including the new data and refitting the model [29]. Obviously, it is not easy to fit the data, unless the number of free parameters is sufficiently large. The same finding has also been reported in our previous study for the $K\Sigma$

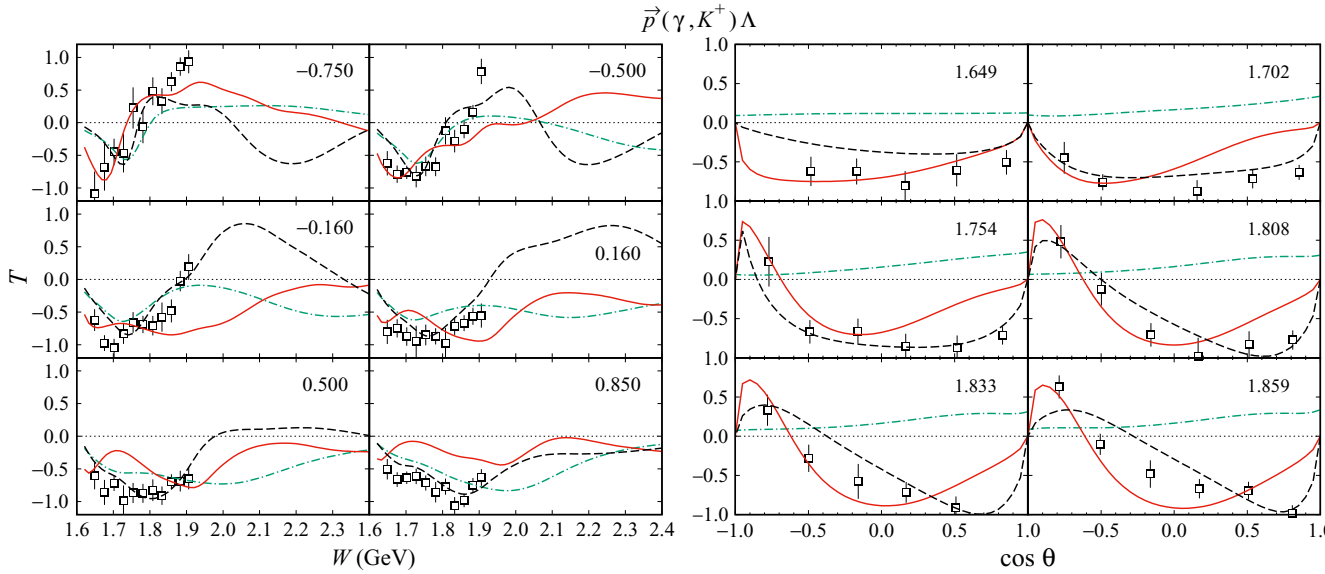

FIG. 8. Target asymmetry as functions of the total c.m. energy and kaon angle. Notation of the curves is as in Fig. 2. Experimental data are from the GRAAL (open squares) [30] Collaboration.

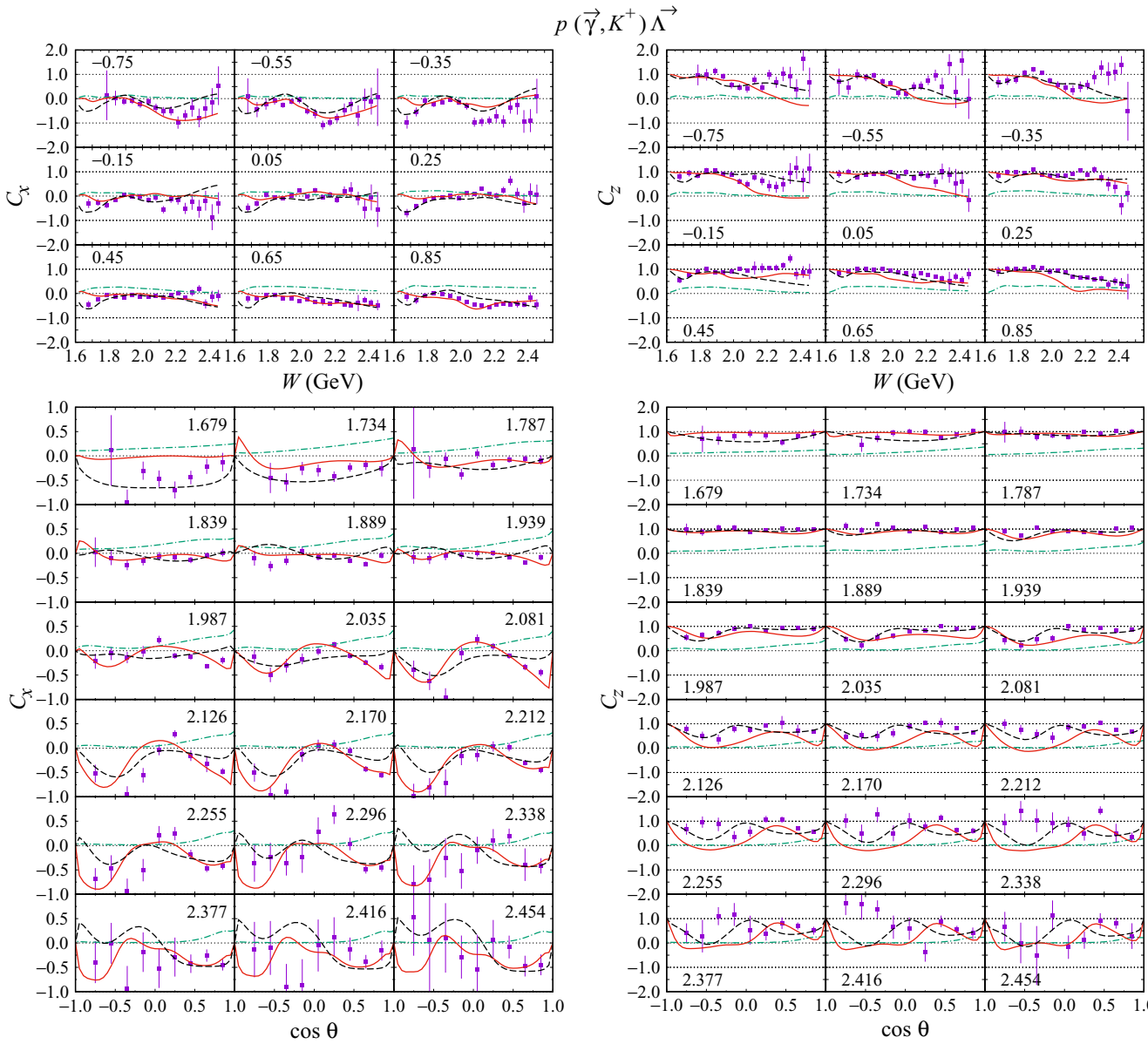

FIG. 9. The beam-recoil double polarization C_x and C_z. Experimental data are from the CLAS Collaboration [32].

photoproduction [12]. With an increase of more than 600 data points in the $K\Sigma$ database the $\chi^2/N_{\rm dof}$ increases from 1.34 to 1.55. The effect seems to be negligible because the data error bars in the case of $K^+\Sigma^0$ photoproduction are relatively larger than in the case of $K^+\Lambda$.

Note that these new data were not available in the previous analysis [1]. As shown in Table II the new data include the recoil polarization P, photon asymmetry Σ, target asymmetry T, and beam-recoil double polarizations O_x and O_z. With limited kinematics these data have been available previously from the LEPS and GRAAL collaborations, respectively, and have been included in the previous discussion in Sec. IV. The double polarization data, however, were given in the recoil frame of reference, i.e., $O_{x'}$ and $O_{z'}$. Therefore, the new observables here extend the database to higher-energy region.

The impact of the new data on the background parameters is shown in Table V, where we can clearly see the decrease of the coupling constant $g_{K\Sigma N}$ and the hadronic form-factor cutoff $\Lambda_{\rm B}$. The latter indicates that to explain the new data the background contribution must be further suppressed. This is shown in Fig. 11, where we can see that the contribution is reduced by nearly 30%. We note that the background decreases as the energy increases because the hadronic form factors have a very soft cutoff. Furthermore, Fig. 11 also reveals that contribution of the background terms at threshold region is significantly suppressed. By comparing this with the result of our study on the $K^+\Lambda$ photoproduction at threshold (see Fig. 2 of Ref. [49]) it is obvious that the background contributions shown in Fig. 11 are smaller. This is understandable because the number of resonances used in the present study is larger

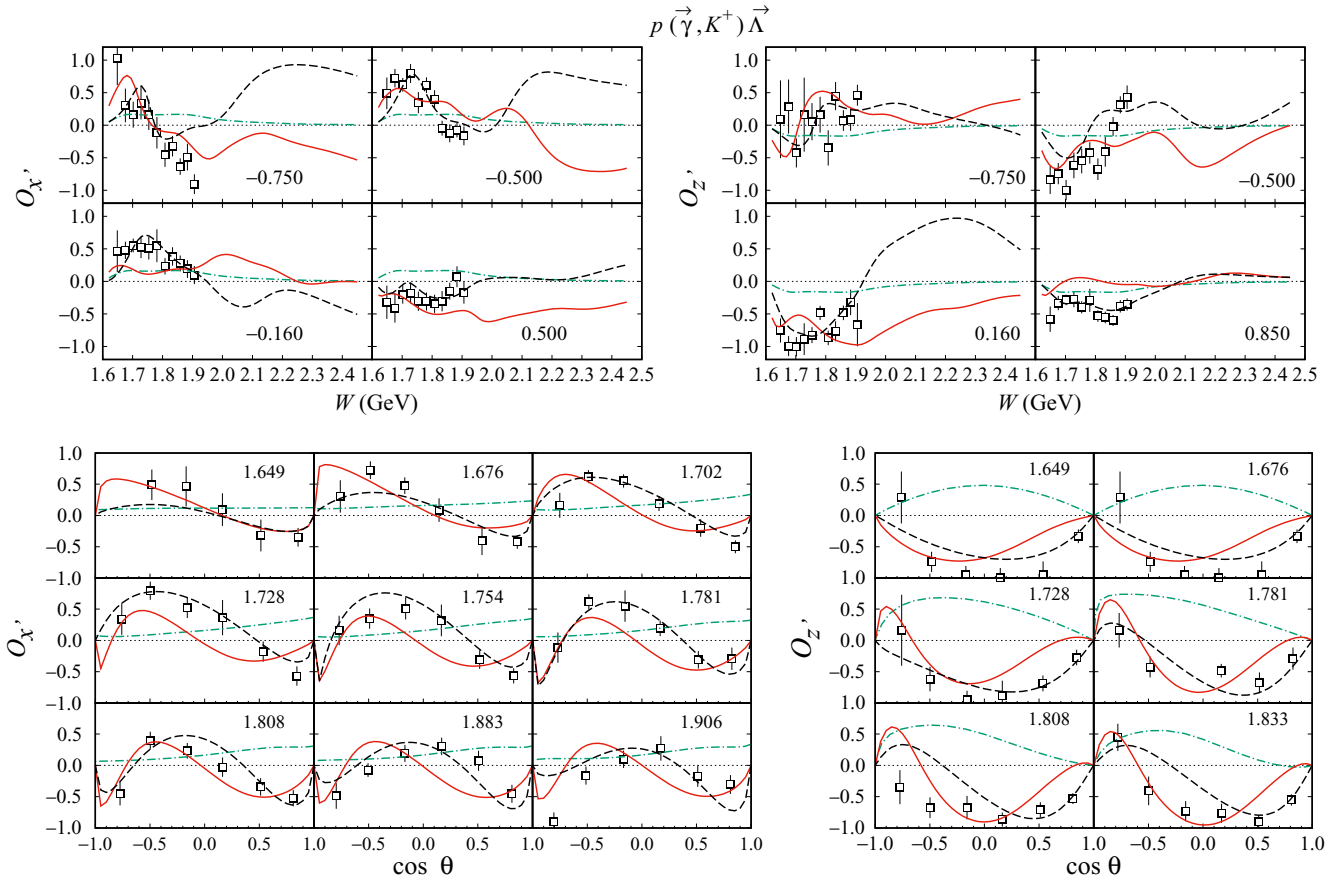

FIG. 10. As in Fig. 9, but for the $O_{x'}$ and $O_{z'}$. Experimental data are from the GRAAL Collaboration [33].

than in the previous one and a number of them have masses near the $K^+\Lambda$ threshold, whereas in the previous study only the $N(1650)S_{11}$ resonance was used. In the present study contributions of the resonances near the threshold region must be compensated with a smaller background.

The suppression of the hadronic form-factor cutoff in the background terms after including the new data has been also observed in our recent study of $K\Sigma$ photoproduction (see Table X of Ref. [12]). However, since in the latter a number of coupling constants also increase and there exist four isospin channels for the $K\Sigma$ photoproduction, different effects are observed in each channel. Nevertheless, in all cases the background contributions are at the same order of magnitude.

The increase of $\chi^2/N_{\rm dof}$ value after including the new data, as shown in Table V, is expected because this result corroborates the previous observations [12,29]. Since including the new CLAS data in the database improves the agreement of the model with these data, we would naturally expect the

TABLE V. Extracted background parameters and hadronic cutoff Λ_B from fits to experimental data by excluding (Fit 1) and including (Fit 2) the new CLAS 2016 data [29]). Note that $N_{\rm dof} = N_{\rm data} - N_{\rm par.}$.

Parameter	Fit 1	Fit 2
$g_{K\Lambda N}/\sqrt{4\pi}$	−3.00	−3.00
$g_{K\Sigma N}/\sqrt{4\pi}$	1.30	0.90
$G^V_{K*}/4\pi$	−0.10	0.37
$G^T_{K*}/4\pi$	−0.04	−0.62
$G^V_{K_1}/4\pi$	0.95	0.01
$G^T_{K_1}/4\pi$	0.41	−0.16
Λ_B	0.62	0.58
$N_{\rm data}$	7433	9003
$N_{\rm par.}$	141	141
$\chi^2/N_{\rm dof}$	1.63	2.88

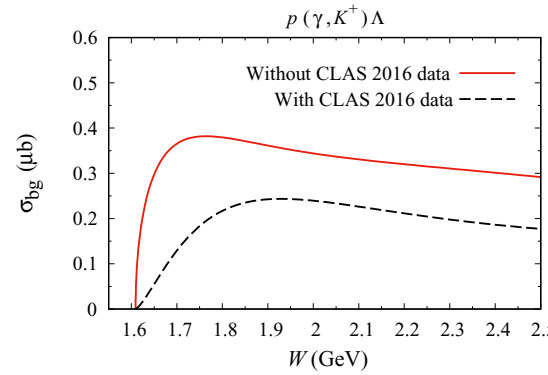

FIG. 11. Contribution of the background amplitude to the calculated total cross section for the models fit with and without the new CLAS 2016 data.

TABLE VI. The extracted nucleon resonance parameters from fits to experimental data without (Fit 1) and with (Fit 2) the new CLAS 2016 data [29]. The uncertainties in the extracted parameter values are merely obtained from MINUIT [41]. The parameters that are significantly influenced by the new data are written with boldface fonts. The last column is obtained by using Eq. (2).

Resonance (PDG status)	Data from	M_R (MeV)	Γ_R (MeV)	β_K (10^{-3})	$A_{1/2}(p)$ (10^{-3} GeV$^{-1/2}$)	$A_{3/2}(p)$ (10^{-3} GeV$^{-1/2}$)	ϕ (deg.)	$\Delta\chi^2$
$N(1650)S_{11}$	Fit 1	1670 ± 0	114 ± 0	150 ± 5	66 ± 0		95 ± 1	48.6
(****)	Fit 2	1670 ± 0	114 ± 0	**67 ± 0**	**85 ± 0**		**225 ± 0**	42.2
$N(1895)S_{11}$	Fit 1	1880 ± 0	125 ± 1	230 ± 63	14 ± 0		205 ± 2	3.9
(**)	Fit 2	**1910 ± 0**	125 ± 0	**130 ± 70**	**7 ± 0**		**267 ± 1**	0.5
$N(1710)P_{11}$	Fit 1	1680 ± 3	433 ± 18	20 ± 1	33 ± 1		167 ± 2	9.6
(***)	Fit 2	1680 ± 0.1	488 ± 1	20 ± 0	60 ± 1		**232 ± 0**	14.5
$N(1880)P_{11}$	Fit 1	1915 ± 1.2	170 ± 0.9	3 ± 0	17 ± 0		191 ± 3	5.4
(**)	Fit 2	1915 ± 0.8	**280 ± 8**	3 ± 0	17 ± 0		**0 ± 0**	0.3
$N(2300)P_{11}$	Fit 1	2281 ± 4	260 ± 15	11 ± 1	47 ± 2		266 ± 3	5.0
(**)	Fit 2	2270 ± 0	**440 ± 4**	**40 ± 2**	**72 ± 0**		**360 ± 0**	8.4
$N(1720)P_{13}$	Fit 1	1748 ± 2	309 ± 4	40 ± 0	75 ± 1	120 ± 0	191 ± 1	48.5
(***)	Fit 2	1737 ± 0	**197 ± 1**	40 ± 0	65 ± 0	120 ± 0	**289 ± 0**	44.3
$N(1900)P_{13}$	Fit 1	1973 ± 1	320 ± 1	100 ± 0	41 ± 0	−88 ± 1	174 ± 0	76.7
(***)	Fit 2	**1899 ± 1**	320 ± 0	100 ± 0	11 ± 0	−95 ± 0	**291 ± 0**	84.4
$N(1700)D_{13}$	Fit 1	1650 ± 1	100 ± 2	14 ± 1	−10 ± 1	5 ± 1	360 ± 0	4.2
(***)	Fit 2	**1750 ± 1**	**237 ± 2**	16 ± 0	**−3 ± 0**	**−40 ± 1**	**232 ± 0**	4.9
$N(1875)D_{13}$	Fit 1	1920 ± 9	757 ± 21	4 ± 0	15 ± 3	−14 ± 1	84 ± 6	3.8
(***)	Fit 2	**1820 ± 3**	**957 ± 21**	4 ± 0	**28 ± 1**	−14 ± 0	**108 ± 1**	0.3
$N(2120)D_{13}$	Fit 1	2163 ± 2	314 ± 4	8 ± 0	170 ± 1	90 ± 0	68 ± 1	10.9
(***)	Fit 2	2166 ± 1	**285 ± 1**	3 ± 0	168 ± 1	96 ± 1	**258 ± 0**	14.6
$N(1675)D_{15}$	Fit 1	1680 ± 0	105 ± 0	46 ± 6	10 ± 0	10 ± 0	195 ± 1	4.6
(****)	Fit 2	1680 ± 0	105 ± 0	**6 ± 1**	**32 ± 1**	**6 ± 0**	**320 ± 0**	4.9
$N(2060)D_{15}$	Fit 1	2045 ± 0	500 ± 8	13 ± 0	53 ± 3	70 ± 1	83 ± 2	13.5
(**)	Fit 2	2045 ± 0	500 ± 1	10 ± 0	53 ± 4	**20 ± 0**	**236 ± 1**	2.9
$N(2570)D_{15}$	Fit 1	2555 ± 4	333 ± 1	21 ± 1	−17 ± 1	39 ± 0	360 ± 1	5.6
(**)	Fit 2	2550 ± 1	333 ± 1	5 ± 0	**28 ± 0**	**18 ± 0**	**188 ± 1**	0.6
$N(1680)F_{15}$	Fit 1	1690 ± 1	112 ± 9	0 ± 0	−16 ± 0	121 ± 20	86 ± 13	0.0
(**)	Fit 2	1690 ± 1	**124 ± 2**	0 ± 0	−16 ± 0	121 ± 20	**360 ± 1**	0.3
$N(1860)F_{15}$	Fit 1	1954 ± 3	115 ± 3	8 ± 0	8 ± 0	70 ± 1	222 ± 2	10.7
(**)	Fit 2	1960 ± 0	115 ± 0	9 ± 0	8 ± 0	70 ± 1	**350 ± 0**	19.7
$N(2000)F_{15}$	Fit 1	2150 ± 1	385 ± 18	6 ± 1	40 ± 1	36 ± 1	22 ± 3	3.0
(**)	Fit 2	2150 ± 0	380 ± 5	**2 ± 0**	40 ± 0	36 ± 0	**234 ± 0**	6.6
$N(1990)F_{17}$	Fit 1	1920 ± 1	470 ± 1	2 ± 0	28 ± 0	70 ± 1	251 ± 1	6.2
(**)	Fit 2	1920 ± 1	470 ± 1	1 ± 0	**56 ± 0**	**46 ± 0**	**319 ± 1**	1.9
$N(2190)G_{17}$	Fit 1	2140 ± 3	220 ± 2	5 ± 0	−62 ± 3	43 ± 2	256 ± 2	6.4
(***)	Fit 2	**2200 ± 0**	**265 ± 5**	**3 ± 0**	**−73 ± 11**	42 ± 1	**355 ± 1**	7.7
$N(2250)G_{19}$	Fit 1	2272 ± 15	438 ± 29	100 ± 4	0 ± 0	10 ± 0	165 ± 4	3.2
(****)	Fit 2	**2200 ± 1**	**736 ± 27**	100 ± 11	**5 ± 0**	**−10 ± 0**	**131 ± 1**	0.2
$N(2220)H_{19}$	Fit 1	2200 ± 1	500 ± 11	100 ± 1	−10 ± 0	10 ± 0	220 ± 1	6.6
(****)	Fit 2	2200 ± 0	**350 ± 1**	100 ± 2	**12 ± 0**	**−5 ± 0**	227 ± 0	11.1
$N(2600)I_{1,11}$	Fit 1	2750 ± 6	800 ± 26	5 ± 1	18 ± 3	−2 ± 0	111 ± 5	0.4
(***)	Fit 2	2750 ± 2	800 ± 14	**2 ± 0**	18 ± 4	**8 ± 0**	126 ± 2	1.2
$N(2700)K_{1,13}$	Fit 1	2567 ± 1	1050 ± 9	100 ± 8	−5 ± 0	13 ± 0	225 ± 1	7.4
(***)	Fit 2	**2650 ± 5**	**788 ± 23**	100 ± 4	**2 ± 0**	**−7 ± 0**	**282 ± 1**	2.6

deficiency of the model in other kinematics or observables, e.g., the differential cross section.

The influence of the new data on the resonance properties is shown in Table VI. As in the previous study of $K\Sigma$ channels we can see in Table VI that the higher mass resonances are more affected by the new data. This happens because at low energies data had been already available for photon asymmetry Σ and double polarizations $O_{x'}$ and $O_{z'}$. Therefore, the previous model (Fit 1) does not have a problem to reproduce the new data at the low-energy region.

Of course, there is also a resonance with a lighter mass which is significantly affected by the new data, i.e., the $N(1700)D_{13}$ resonance. This can be understood as a result of rearrangement of free parameters to reproduce the fitted data. Note that the determination of the significantly affected resonances given in Table VI is somewhat qualitative because

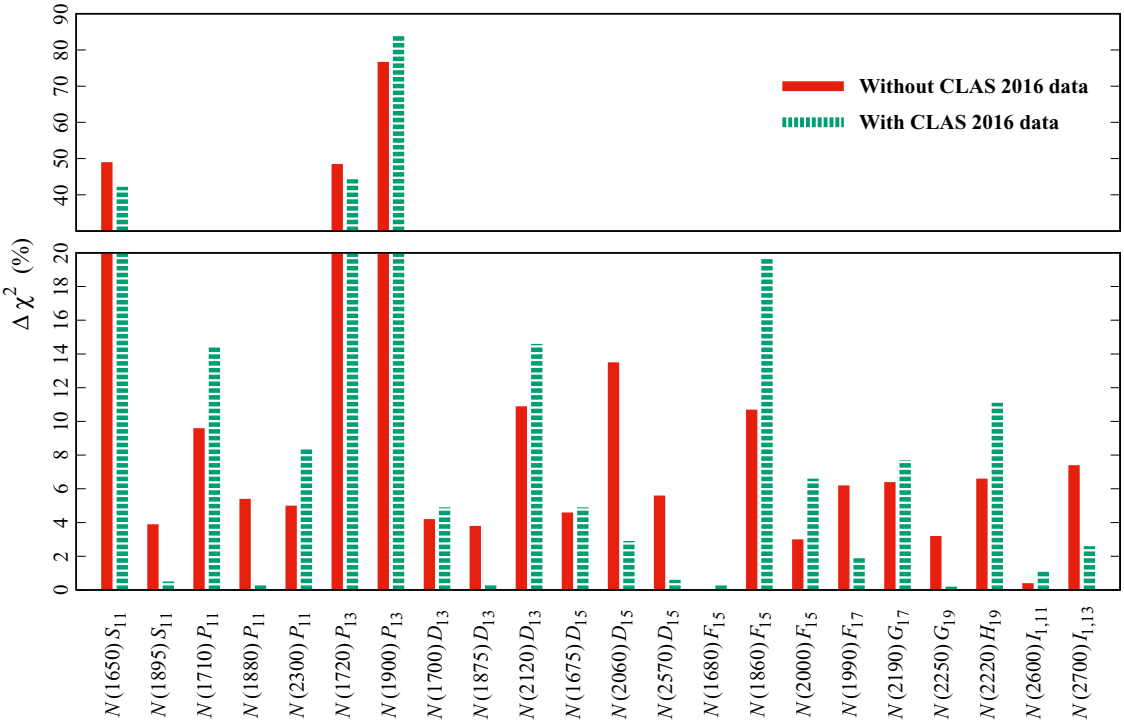

FIG. 12. As in Fig. 1, but for the solutions obtained by excluding (Fit 1) and including (Fit 2) the new CLAS 2016 data [29].

the upper- and lower-bound limits of resonance parameters used during the fit are mostly dictated by the PDG uncertainties and, therefore, it is different from one resonance to another. As a result, the criterion of most affected parameter is also different from one resonance to another. Specifically, we notice that the $N(1895)S_{11}$, $N(1875)D_{13}$, $N(1900)P_{13}$, $N(2190)G_{17}$, $N(2250)G_{19}$, and $N(2700)K_{1,13}$ resonances are the most affected ones. Except for the $N(1900)P_{13}$ resonance, the affected resonances in this work ($K^+\Lambda$ channel) are different from those in the previous work ($K\Sigma$ channels) [12].

As in the previous section the role of each resonance in the process after including the new data can be estimated by using Eq. (2). The result (Fit 2) is listed in the last column of Table VI, where the result obtained from fit without the new data (Fit 1) is also displayed for comparison. This comparison is pictorially displayed in Fig. 12.

Figure 12 clearly exhibits that the inclusion of the new CLAS 2016 data in our present work does not change the result and the conclusion of the three most important nucleon resonances, i.e., the $N(1650)S_{11}$, $N(1720)P_{13}$, and $N(1900)P_{13}$ states, in the $\gamma p \to K^+\Lambda$ process drawn in the previous section. For the $N(1900)P_{13}$ the value of $\Delta\chi^2$ becomes even larger. This result provides a strong support for the recent proposal to raise the rating of this resonance to four star [50]. Interestingly, however, the $N(1710)P_{11}$ resonance, which was also proposed in Ref. [50] and has received a four-star rating in the 2016 PDG listing [9], is found to be less important in the present work. As shown in Fig. 12 its role in suppressing the χ^2 in the $K^+\Lambda$ photoproduction is less important compared with the $N(1860)F_{15}$ state. In our previous analysis for the $K^+\Lambda$ channel the $N(1710)P_{11}$ resonance is found to be much less important (see Fig. 2 of Ref. [1] and Fig. 7 of Ref. [44]). However, this resonance is presumably required to explain the threshold data of the $K\Sigma$ photoproduction [12].

Comparison between the calculated observables and the new CLAS 2016 data is exhibited in Figs. 13–15. The improvement made in the recoil polarization observable after including the new data shown in Fig. 13 is obviously not significant, because data with small error bars from threshold up to 2.8 GeV have been available for this observable before 2016 and, therefore, the previous model (Fit 1) can easily reproduce them.

At some kinematics, e.g., at $\cos\theta \approx -0.5$, the previous model (Fit 1) shows even a better performance, whereas the result after fitting the new data (Fit 2) is shifted from the data. We believe that this phenomenon originates from the effect of other observables in the new data, i.e., the T, O_x, and O_z, for which the fit has to compromise with the extreme changes at this kinematics to explain these data.

In the case of photon asymmetry the discrepancy between the calculated observables of previous model (Fit 1) and experimental data gets larger as the energy increases. This result is also expected because low-energy data of this observable have been previously available from the GRAAL Collaboration [30] (see the lower panel of Fig. 13) and the previous model was fit to these data. This discrepancy becomes very significant at $2 \lesssim W \lesssim 2.18$ GeV. As a consequence, fitting these new data will significantly affect the resonances whose masses are within this energy range, as has been discussed above.

The same behavior is also shown by the target asymmetry as displayed in the upper panel of Fig. 14. Near the threshold

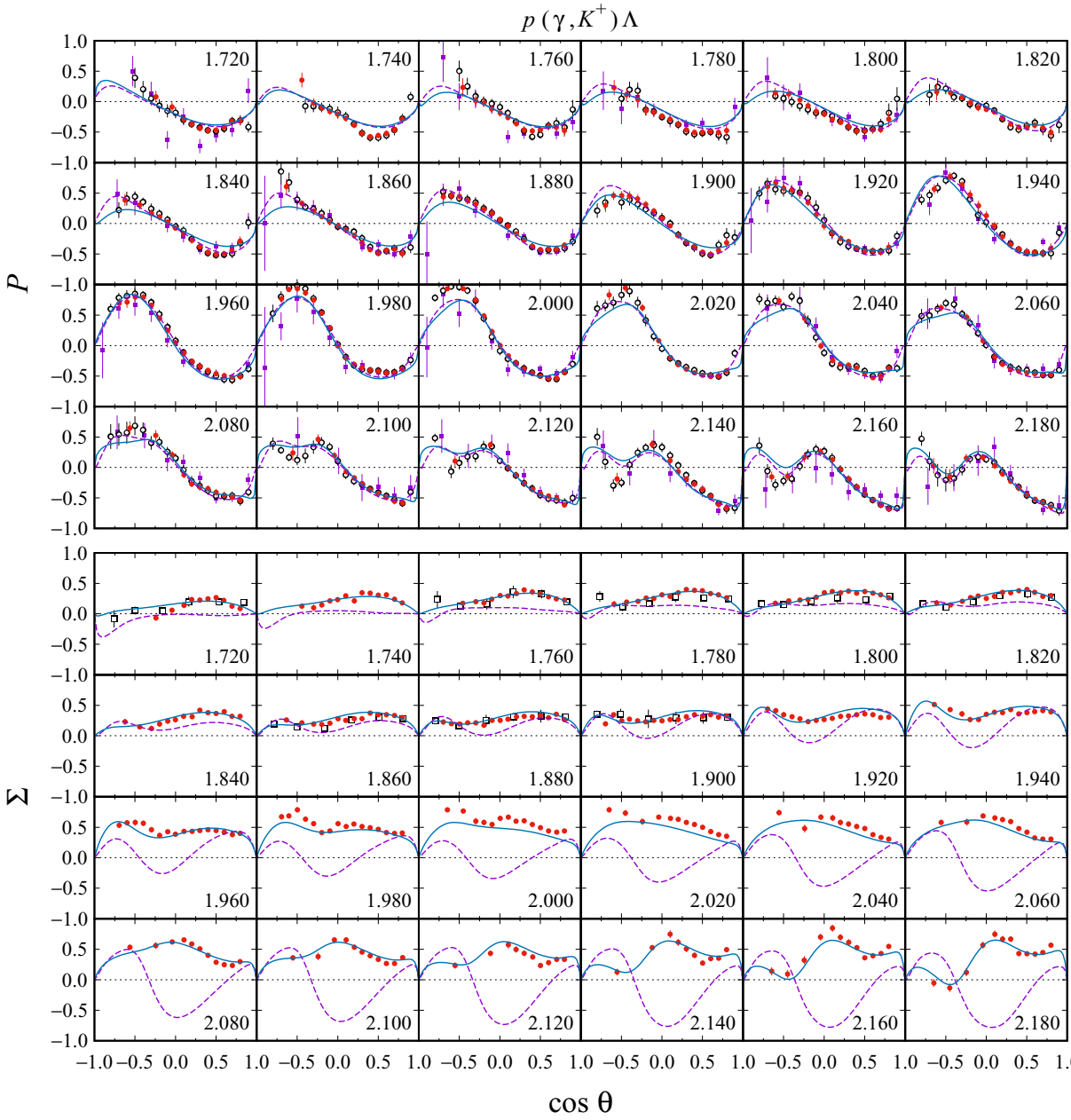

FIG. 13. Angular distributions of the recoil polarization P and photon asymmetry Σ. The dashed and solid lines are obtained from the models fit without and with the new CLAS 2016 data, respectively. Experimental data are from the CLAS 2016 (solid circles [29]), CLAS 2006 (solid squares [4]), CLAS 2010 (open circles [5]), and GRAAL 2007 (open squares [30]) collaborations. The corresponding total c.m. energy W in unit of GeV is shown in each panel.

small discrepancy is shown by the new CLAS and GRAAL data. At lower energies the prediction of the two models is certainly closer to the GRAAL data, especially that of Fit 2. At higher energies the discrepancy between Fit 1 and Fit 2 becomes more apparent, especially at $\cos\theta \approx -0.5$, where the fit must dramatically change the value of T. This is the origin of the changes in the resonance parameters after including the new data as previously shown in Table VI. It is also important to note that in contrast to the cases of recoil polarization and photon asymmetry shown in Fig. 13, where fitting the new data leads to a perfect agreement over a wide range of kinematics, in the case of target asymmetry both models seem to be difficult to explain the forward angle data with $W \gtrsim 2.14$ GeV. We believe that further study in the future is required to relieve this problem.

The performance of both models in explaining the beam-recoil double polarization observables O_x and O_z is shown in Figs. 14 and 15. The GRAAL data $O_{x'}$ and $O_{z'}$ are also shown

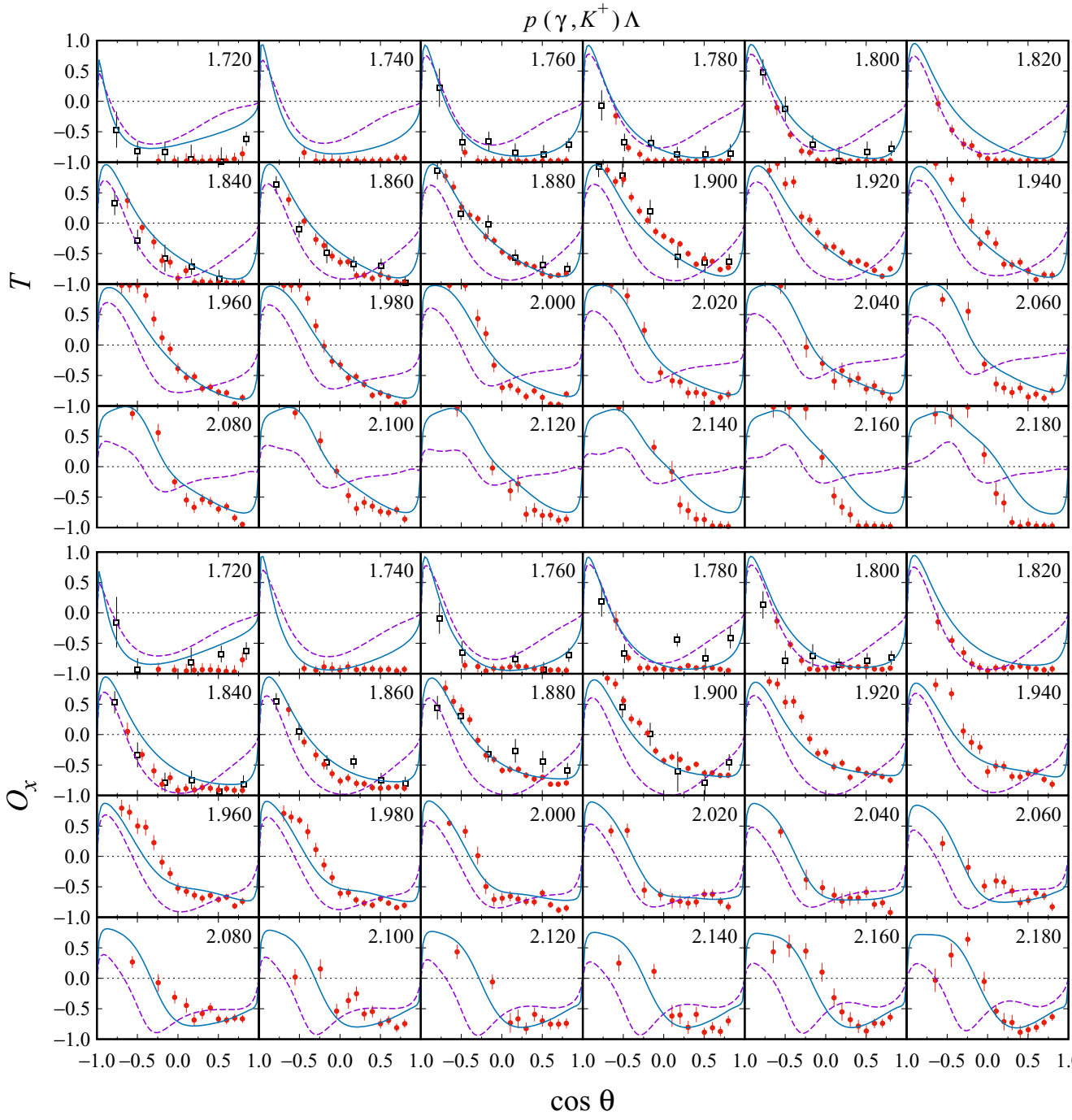

FIG. 14. As in Fig. 13, but for the angular distributions of target asymmetry T and photon-recoil double polarization O_x.

for comparison, where we have used the transformation [35]

$$\begin{pmatrix} O_x \\ O_z \end{pmatrix} = \begin{pmatrix} \cos\theta & \sin\theta \\ -\sin\theta & \cos\theta \end{pmatrix} \begin{pmatrix} O_{x'} \\ O_{z'} \end{pmatrix}. \tag{3}$$

Figures 14 and 15 indicate that within their error bars the two data sets are consistent and fitting the new data greatly improve the agreement with the data, especially at $W \gtrsim 1.92$ GeV, where data were previously not available. At this energy region and $\cos\theta \approx -0.5$ the variance between calculated O_x observables obtained from Fit 1 and Fit 2 is large and, therefore, also responsible for the changes of the nucleon resonance properties as shown in Table VI and discussed above.

VI. SUMMARY AND CONCLUSION

We have studied kaon photoproduction on the proton, $\gamma p \to K^+\Lambda$ by using the multipoles approach. The main motivation of this study was to provide an update to our previous model that used very limited experimental data and out-of-date information on nucleon resonances. To that end we added the

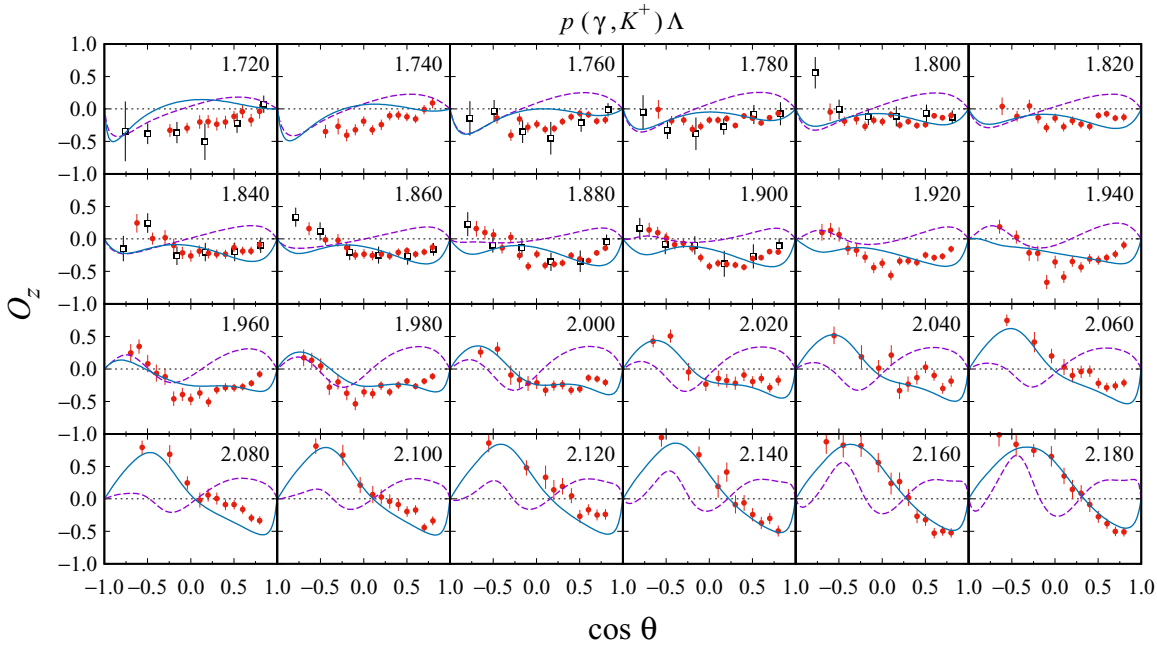

FIG. 15. As in Fig. 13, but for the photon-recoil double polarization O_z.

recently available kaon photoproduction data, including the new CLAS 2016 data, in the fitting database. The present database contains four times more data points than the previous one. Information on the nucleon resonances recently provided by PDG was used as an input to our model. By fitting the calculated observables to nearly 7400 experimental data points and constraining the resonance parameters within the error bars provided by PDG we obtained a chi-squared per degrees of freedom of 1.63, i.e., the model can nicely reproduce the data. As in our previous works, contribution of the $N(1710)P_{11}$ state to the $K^+\Lambda$ photoproduction was found to be relatively small. In the resonance sector, the most important contributors in the present model are the $N(1650)S_{11}$, $N(1720)P_{13}$, and $N(1900)P_{13}$ resonances. The present finding is substantially different compared with the result of our previous study, where the three most important resonances were the $N(1900)F_{17}$, $N(1675)D_{15}$, and $N(1900)P_{13}$. Except the recoil polarization observable P, all observables in the new CLAS 2016 data could not be reproduced by the present model, unless the new data were included in the fitting database and the model was refitted. The inclusion of the new data increases the chi-squared per degrees of freedom from 1.63 to 2.88. Nonetheless, the latter does not change our conclusion on the importance of the $N(1650)S_{11}$, $N(1720)P_{13}$, and $N(1900)P_{13}$ resonances in the kaon photoproduction process. In general, the work described in this paper has significantly improved our previous multipoles model.

ACKNOWLEDGMENT

This work has been partly supported by the University of Indonesia through the Hibah PITTA UI program.

[1] T. Mart and A. Sulaksono, Phys. Rev. C **74**, 055203 (2006).
[2] Online version is available in T. Mart, C. Bennhold, H. Haberzettl, and L. Tiator, http://www.kph.uni-mainz.de/MAID/kaon/kaonmaid.html. The published versions include T. Mart and C. Bennhold, Phys. Rev. C **61**, 012201 (1999); T. Mart, *ibid.* **62**, 038201 (2000); C. Bennhold, H. Haberzettl, and T. Mart, arXiv:nucl-th/9909022.
[3] K. H. Glander *et al.* (SAPHIR Collaboration), Eur. Phys. J. A **19**, 251 (2004); M. Q. Tran *et al.*, Phys. Lett. B **445**, 20 (1998).
[4] R. Bradford *et al.* (CLAS Collaboration), Phys. Rev. C **73**, 035202 (2006).
[5] M. E. McCracken *et al.* (CLAS Collaboration), Phys. Rev. C **81**, 025201 (2010).
[6] T. C. Jude *et al.* (Crystal Ball at MAMI Collaboration), Phys. Lett. B **735**, 112 (2014).
[7] M. Sumihama *et al.* (LEPS Collaboration), Phys. Rev. C **73**, 035214 (2006).
[8] S. Eidelman *et al.* (Particle Data Group Collaboration), Phys. Lett. B **592**, 1 (2004).
[9] C. Patrignani *et al.* (Particle Data Group Collaboration), Chin. Phys. C **40**, 100001 (2016).
[10] S. Sakinah and T. Mart, in 2^{nd} *International Symposium on Current Progress in Mathematics and Sciences, Universitas Indonesia, Depok, 2016*, AIP Conf. Proc. (to be published).
[11] T. Mart, S. Clymton, and A. J. Arifi, Phys. Rev. D **92**, 094019 (2015).
[12] T. Mart and M. J. Kholili (unpublished).
[13] D. Drechsel, O. Hanstein, S. S. Kamalov, and L. Tiator, Nucl. Phys. A **645**, 145 (1999).
[14] R. A. Adelseck and B. Saghai, Phys. Rev. C **42**, 108 (1990).

[15] K. A. Olive *et al.* (Particle Data Group Collaboration), Chin. Phys. C **38**, 090001 (2014).
[16] A. V. Anisovich, R. Beck, E. Klempt, V. A. Nikonov, A. V. Sarantsev, and U. Thoma, Eur. Phys. J. A **48**, 15 (2012).
[17] R. L. Workman, M. W. Paris, W. J. Briscoe, and I. I. Strakovsky, Phys. Rev. C **86**, 015202 (2012).
[18] G. Höhler *et al.*, Physik Daten **12**, 1 (1979).
[19] V. Shklyar and H. Lenske, Phys. Rev. C **87**, 015201 (2013).
[20] V. Sokhoyan *et al.*, Eur. Phys. J. A **51**, 95 (2015).
[21] A. W. Hendry, Phys. Rev. Lett. **41**, 222 (1978).
[22] R. A. Arndt, I. I. Strakovsky, and R. L. Workman, Phys. Rev. C **53**, 430 (1996).
[23] V. A. Nikonov, A. V. Anisovich, E. Klempt, A. V. Sarantsev, and U. Thoma, Phys. Lett. B **662**, 245 (2008).
[24] M. Shrestha and D. M. Manley, Phys. Rev. C **86**, 055203 (2012).
[25] G. Penner and U. Mosel, Phys. Rev. C **66**, 055212 (2002).
[26] R. L. Crawford and W. T. Morton, Nucl. Phys. B **211**, 1 (1983).
[27] R. E. Cutkosky, C. P. Forsyth, R. E. Hendrick, and R. L. Kelly, Phys. Rev. D **20**, 2839 (1979).
[28] K. Fujii *et al.*, Nucl. Phys. B **197**, 365 (1982).
[29] C. A. Paterson *et al.*, Phys. Rev. C **93**, 065201 (2016).
[30] A. Lleres *et al.* (GRAAL Collaboration), Eur. Phys. J. A **31**, 79 (2007).
[31] K. Hicks *et al.*, Phys. Rev. C **76**, 042201 (2007).
[32] R. Bradford *et al.*, Phys. Rev. C **75**, 035205 (2007).
[33] A. Lleres *et al.* (GRAAL Collaboration), Eur. Phys. J. A **39**, 149 (2009).
[34] A. M. Sandorfi, B. Dey, A. Sarantsev, L. Tiator, and R. Workman, AIP Conf. Proc. **1432**, 219 (2012).
[35] A. M. Sandorfi, S. Hoblit, H. Kamano, and T.-S. H. Lee, J. Phys. G **38**, 053001 (2011).
[36] H. Kamano, S. X. Nakamura, T.-S. H. Lee, and T. Sato, Phys. Rev. C **88**, 035209 (2013).
[37] D. Skoupil and P. Bydzovský, Phys. Rev. C **93**, 025204 (2016).
[38] T. Mart and N. Nurhadiansyah, Few-Body Syst. **54**, 1729 (2013).
[39] R. A. Adelseck and L. E. Wright, Phys. Rev. C **38**, 1965 (1988).
[40] L. Syukurilla and T. Mart, Int. J. Mod. Phys. E **24**, 1550008 (2015); T. Mart and A. K. Sari, Mod. Phys. Lett. A **28**, 1350054 (2013).
[41] F. James and M. Roos, Comput. Phys. Commun. **10**, 343 (1975).
[42] B. Julia-Diaz, B. Saghai, T. S. H. Lee, and F. Tabakin, Phys. Rev. C **73**, 055204 (2006).
[43] L. De Cruz, T. Vrancx, P. Vancraeyveld, and J. Ryckebusch, Phys. Rev. Lett. **108**, 182002 (2012).
[44] T. Mart and M. J. Kholili, Phys. Rev. C **86**, 022201(R) (2012).
[45] V. Pascalutsa and R. Timmermans, Phys. Rev. C **60**, 042201 (1999).
[46] T. Mart and B. I. S. van der Ventel, Phys. Rev. C **78**, 014004 (2008); T. Mart, Nucl. Phys. A **815**, 18 (2009); T. Mart, L. Tiator, D. Drechsel, and C. Bennhold, *ibid.* **640**, 235 (1998); T. Mart, D. Kusno, C. Bennhold, L. Tiator, and D. Drechsel, *ibid.* **631**, 765 (1998); A. Salam, T. Mart, and K. Miyagawa, Few Body Syst. **54**, 261 (2013); K. Miyagawa, T. Mart, C. Bennhold, and W. Glockle, Phys. Rev. C **74**, 034002 (2006); H. Yamamura, K. Miyagawa, T. Mart, C. Bennhold, W. Glockle, and H. Haberzettl, *ibid.* **61**, 014001 (1999).
[47] T. Mart, Phys. Rev. D **83**, 094015 (2011); **88**, 057501 (2013).
[48] E. Gutz *et al.* (CBELSA/TAPS Collaboration), Eur. Phys. J. A **50**, 74 (2014).
[49] T. Mart, Phys. Rev. C **82**, 025209 (2010).
[50] V. D. Burkert *et al.*, arXiv:1412.0241.